Applied Catalysis B: Environmental 134–135 (2013) 26–33

Contents lists available at SciVerse ScienceDirect

Applied Catalysis B: Environmental

journal homepage: www.elsevier.com/locate/apcatb

In situ growth of gold nanoparticles onto polydopamine-encapsulated magnetic microspheres for catalytic reduction of nitrobenzene

Tao Zeng[a], Xiao-le Zhang[a,b], Hong-yun Niu[a], Yu-rong Ma[a], Wen-hui Li[a], Ya-qi Cai[a,*]

[a] *State Key Laboratory of Environmental Chemistry and Ecotoxicology, Research Center for Eco-Environmental Sciences, Chinese Academy of Sciences, P.O. Box 2871, Beijing 100085, China*
[b] *College of Life Science, Hebei United University, Tangshan, Hebei 063000, China*

ARTICLE INFO

Article history:
Received 27 August 2012
Received in revised form
14 December 2012
Accepted 31 December 2012
Available online 5 January 2013

Keywords:
Gold nanoparticles
Magnetic microspheres
Dopamine
Catalyst
Nitrobenzene

ABSTRACT

A simple and green method for the deposition of gold nanoparticles (Au NPs) on the surface of polydopamine (PDA)-encapsulated Fe_3O_4 nanoparticles is proposed to fabricate a core–shell Fe_3O_4@PDA–Au nanocatalyst. In the current approach, Fe_3O_4 core, about 400 nm in diameter, is enveloped in a PDA coating with a thickness of about 45 nm on which plenty of small Au NPs are immobilized subsequently. PDA serves as a reductant as well as a stabilizer so that additional reagents and thermo treatment are not necessary. In addition, both the size of Au NPs and the thickness of PDA layer are tunable to load more Au NPs with appropriate size on the PDA coating. The Au content on Fe_3O_4@PDA–Au nanocomposites is about 4.3 wt.%, which endows the nanocatalyst with high catalytic performance in the reduction of *o*-nitroaniline to benzenediamine by $NaBH_4$ (with a conversion of 99% in 7 min). Most importantly, the catalyst can be easily recycled by using an external magnetic field due to the high magnetization (39.6 emu g^{-1}) and shows excellent reusability (8 cycles with a conversion of >98% for *o*-nitroaniline). The as-prepared catalyst also show good activity for the reduction of other nitrobenzene analogs. These facilitate the practical application of the catalyst in reduction of nitroaromatic compounds.

1. Introduction

Recently, noble metal nanoparticles have attracted tremendous attention due to their unique optical, catalytic, and electrochemistry properties which endow them with high potentials for a wide range of applications [1–5]. Among them, Au NPs have been proven as a high-efficiency catalyst in a number of oxidation and reduction reactions [6–9]. Generally, nanoparticles in solution exhibit strong tendency to aggregate because of the high surface energy, which leads to the decrease in catalytic activity [10]. To enhance the catalyst stability, Au NPs have been dispersed onto different solid matrices such as carbon nanotube, silica, titania and other metal oxides [11–13]. However, time-consuming separation procedures such as filtration or centrifugation must be performed to isolate these catalysts from the reaction system. To solve the separation problem, magnetic materials can be used as the solid matrix to support Au NPs. Several studies have been reported on the synthesis and application of magnetic materials supported Au nanocatalysts which can be recovered and recycled through a convenient magnetic separation approach [14–18]. Although these composite materials show relatively high catalytic activity and recyclability, the synthesis procedures are somewhat complicated and toxic reagents or heat treatment should be involved. Therefore, development of a simple and low toxic process to synthesize magnetic-Au nanocatalyst has become critical.

In the past decade, a variety of phenol derivatives have been utilized in the synthesis of gold and silver nanoparticles as both reducing agents and stabilizers [19–22]. Dopamine, which is an important natural chemical neurotransmitter present in various animals, has gained extensive concern because of the numerous amine and catechol functional groups and the ability of adhering to almost all material surfaces and autopolymerization to form PDA coating under mild condition [23,24]. The formation of PDA coating is simple, inexpensive and green and the thickness of PDA coating can be readily controlled by changing the experimental parameters. Although the specific chemical composition is not precisely known to date, plenty of catechol groups prone to be oxidized are believed to be present in the PDA coating [25]. Therefore, PDA can be an alternative for the synthesis of metallic nanoparticles due to the apparent reductive and stabilizing capacity [11,25–27]. Studies on one-step generation of Au NPs using PDA as dual roles of reductant and stabilizer have been reported in some literature [28,29]. However, there is only limited research on the loading of Au NPs onto magnetic particles to prepare magnetic-Au nanocatalyst through this approach.

* Corresponding author. Tel.: +86 10 6284 9182; fax: +86 10 6284 9182.
E-mail address: caiyaqi@rcees.ac.cn (Y.-q. Cai).

0926-3373/$ – see front matter © 2013 Elsevier B.V. All rights reserved.
http://dx.doi.org/10.1016/j.apcatb.2012.12.037

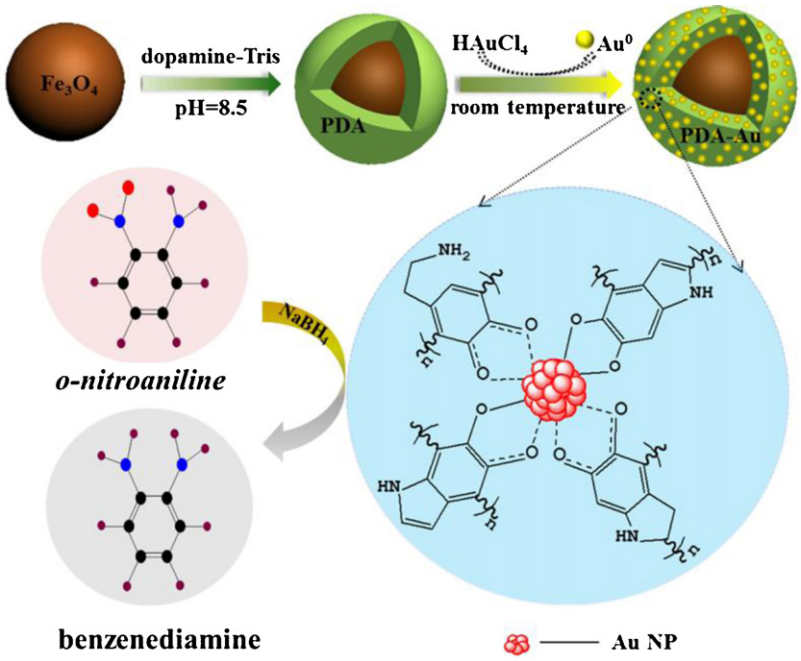

Fig. 1. Schematic diagram of the synthetic strategy, possible mechanism, and application of Fe_3O_4@PDA–Au nanocomposites.

In the present work, we report a facile and green method for the fabrication of magnetically recyclable nanocatalyst with *in situ* growth of Au NPs in the outershell of presynthesized core–shell structured Fe_3O_4@PDA composite (Fig. 1). PDA layer was used as a medium that possesses reducing ability and stabilizing ability for the deposition of Au NPs. Compared with other methods of magnetic-Au heterogeneous catalyst formation, additional toxic reagent or physical treatment is not needed. At the same time, both the size of Au NPs and the thickness of PDA shell are tunable. Moreover, the Au NPs are anchored homogeneously and tightly onto the PDA coating of the Fe_3O_4@PDA magnetic nanoparticles so that the nanocomposite can be easily recycled with an external magnetic field. The Fe_3O_4@PDA–Au nanocomposite was employed in the catalytic reduction of nitrobenzene in the presence of $NaBH_4$ because nitrobenzene compounds are high toxic to human beings and the toxicities of their reduction products, aminoaromatic compounds, are much lower [30]. In addition, the selective hydrogenation of nitroaromatic compounds to the corresponding aminoaromatic compounds is widely used during the chemical processes producing pharmaceuticals, dyes, and polymers [31]. To the best of our knowledge, this is the first report of green-synthesized and well-defined Fe_3O_4@PDA–Au composites using as a highly efficient catalyst system in the reduction of nitrobenzene.

2. Experimental

2.1. Chemicals

Ferric chloride hexahydrate ($FeCl_3{\cdot}6H_2O$), sodium acetate (NaAc), 2-amino-2-hydroxymethylpropane-1,3-diol (Tris), ethylene glycol (EG), trisodium citrate dihydrate, and hydrogen tetrachloroaurate hydrate ($HAuCl_4{\cdot}4H_2O$) were purchased from Sinopharm Chemistry Reagent Co., Ltd. (Beijing, China). *o*-Nitroaniline (*o*-NA), *m*-nitroaniline, *p*-nitroaniline, *o*-nitrotoluene, *m*-nitrotoluene, *p*-nitrophenol, *o*-nitrochlorobenzene, 2,4-dinitrotoluene, 3-hydroxytyramine hydrochloride (dopamine), and sodium hydroxide ($NaBH_4$) were obtained from J&K Chemical Ltd. (Beijing, China). All chemicals were used as received without any further purification. Ultrapure water was prepared by using Milli-Q SP reagent water system (Millipore, Bedford, MA, USA).

2.2. Preparation of Fe_3O_4@PDA–Au nanocatalyst

The magnetic Fe_3O_4 nanoparticles were firstly synthesized through a solvothermal reaction according to the previous report.[32] Briefly, $FeCl_3{\cdot}6H_2O$ (3.24 g), trisodium citrate (0.6 g), and NaAc (3.6 g) were dissoveld in ethylene glycol (60 mL) with magnetic stirring at room temperature for 30 min. The homogeneous yellow solution was then transferred to a Teflon-lined stainless-steel autoclave and sealed to heat at 200 °C. After reaction for 12 h, the autoclave was cooled to room temprature. The obtained Fe_3O_4 NPs were washed with ethanol and deionized water three times, respectively, and then dried under vacuum for 12 h.

To prepare Fe_3O_4@PDA composites, 0.4 g of the as-prepared Fe_3O_4 was dispersed in 200 mL of dopamine–Tris solution (2 mg mL^{-1}, pH 8.5, 10 mM Tris buffer), and allowed to proceed for 24 h under stirring at room temprature. The resultant product was separated and collected with a magnet, followed by washing with deionized water 3 times.

In a typical preparation of Fe_3O_4@PDA–Au, 100 mg of Fe_3O_4@PDA NPs was suspended in $HAuCl_4$ aqueous solution (80 ml) and the mixture was stirred for 24 h at room temprature. The resultant nanocomposite was separated and rinsed with deionized water for at least three times, and then dried under vacuum for further use. To ascertain the loading amount of Au, the catalyst was digested and analyzed by Inductively Coupled Plasma Mass Spectrometry (ICP-MS, Agilent, CA). When the added $HAuCl_4$ concentration was $X \times 10^{-4}$ M, the as-prepared catalyst was denoted as Fe_3O_4@PDA–Au_X. Unless otherwise specified, the Fe_3O_4@PDA@Au in the article refers to Fe_3O_4@PDA@Au_6.

2.3. Catalytic reduction of nitrobenzene

The reduction of *o*-NA with $NaBH_4$ was carried out to examine the catalytic activity and reusability of the Fe_3O_4@PDA–Au catalysts. Amounts of 2 mL of deionized water, 0.25 mL of *o*-NA aqueous

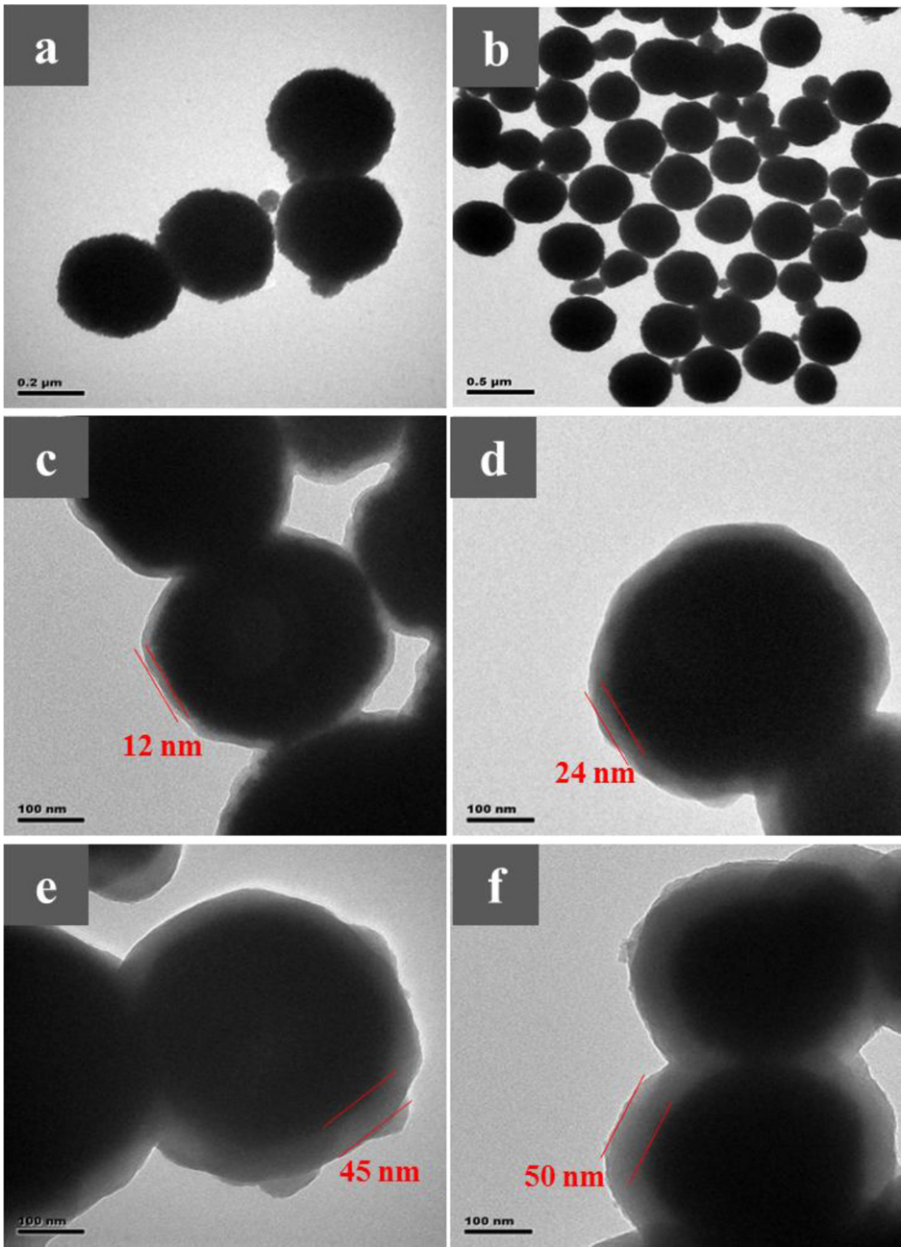

Fig. 2. TEM images of the as-prepared Fe_3O_4 NPs (a, b) and the core–shell structured Fe_3O_4@PDA composites with a varying thickness of polydopamine shell by changing reaction time from 6 h (c) to 12 h (d), 24 h (e), and 48 h (f), respectively.

solution (3.4×10^{-3} M), and 0.25 mL of fresh $NaBH_4$ (1.2 M) were added into a quartz cuvette in sequence, followed by additon of 0.05 mL of catalyst (1 mg mL^{-1}) to the mixture. The color of the solution gradually vanished as the reaction proceeded. The reaction progress was monitored by ultraviolet–visible (UV–vis) spectrometry at a certain time interval to obtain successive information. After the whole reduction process was completed, the catalysts were separated from the mixture with a magnet and then reused in the next cycle. The catalytic reduction of other nitrobenzenes were conducted under the same condition of *o*-NA. The conversions were determined by the gas chromatography/mass spectroscopy (GC/MS) analysis.

2.4. Characterization

UV–vis spectra were recorded by DU 800 nucleic acid/protein analyzer (Beckman Instruments, Inc., Rosemead, CA). The size and structure of nanoparticles were surveyed by H-7500 transmission electronic microscopy (Hitachi, Tokyo, Japan) operating at 80 kV accelerated voltage. The elemental composition of Fe_3O_4@PDA–Au composites was analyzed by employing an S-2400 scanning electron microscopy-energy dispersive X-ray spectrometry (SEM-EDX, Hitachi, Tokyo, Japan). X-ray diffraction studies (XRD, PANalytical X' Pert diffractometer, Almelo, Netherlands) were performed by using a monochromatized X-ray beam with nickel-filtered Cu Kα radiation with 0.4° min^{-1} scan rate. X-Ray photoelectron spectroscopy (XPS) measurements were conducted by applying an ESCA-Lab-200i-XL spectrometer (Thermo Scientific, Waltham, MA) with monochromatic Al Kα radiation (1486.6 eV). FTIR spectra were taken in KBr pressed pellets on a NEXUS 670 Infrared Fourier Transform Spectrometer (Nicolet Thermo, Waltham, MA). The magnetization curves of the products were measured with a vibrating sample magnetometer (VSM, LDJ9600, Troy, MI).

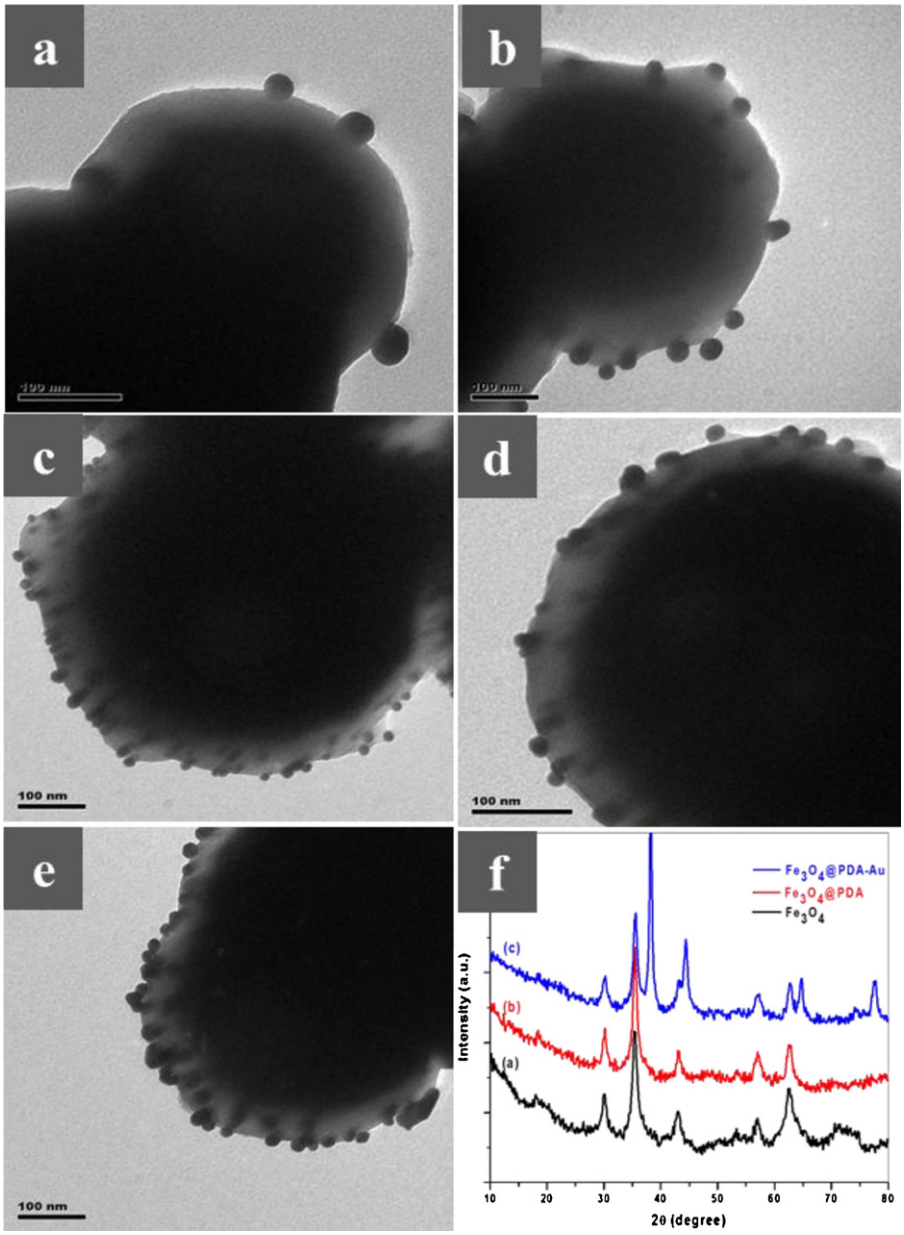

Fig. 3. TEM images of Fe_3O_4@PDA–Au nanocomposites with a different dosages of $HAuCl_4$: (a) 3×10^{-4} M (Fe_3O_4@PDA–Au_3), (b) 4.5×10^{-4} M (Fe_3O_4@PDA–$Au_{4.5}$), (c) 6×10^{-4} M (Fe_3O_4@PDA–Au_6), (d) 9×10^{-4} M (Fe_3O_4@PDA–Au_9), and (e) 12×10^{-4} M (Fe_3O_4@PDA–Au_{12}). XRD patterns (f) of the as-prepared Fe_3O_4 (black), Fe_3O_4@PDA (red), and Fe_3O_4@PDA–Au (blue).

3. Results and discussion

Fig. 2 shows the TEM images of the as-prepared nanoparticles. From Fig. 2a and b, it can be found that the monodisperse Fe_3O_4 NPs possess uniformly spherical shape with a rough surface and an approximate diameter of 400 nm. The magnetic particles exhibit excellent dispersibility and stability in water solution (Fig. S1) due to the presence of the citrate groups modified on the surface, which favors the subsequent coating with PDA layer.

PDA layer with good stability was formed onto the Fe_3O_4 NPs surfaces through autopolymerization of dopamine and Tris buffer was employed to adjust the solution pH according to previous reference [23]. The exact polymerization mechanism of dopamine is still unclear. The prevalent view is that in alkaline conditions dopamine is oxidized to dopaminequinone which subsequently cyclizes to leukodopaminechrome. Next, 5,6-dihydroxyindole is obtained through a series of oxidation and rearrangement and polymerize *via* aryl-aryl and aryl-indolyl linkages to form PDA (Fig. S2). The adhesion of PDA onto Fe_3O_4 surface may attribute to the formation of $-COO^-H_3N^+-$ ion pairs between the abundant carboxyl groups on the particle surface and the amine groups of dopamine [33]. In addition, the hydroxyl groups on the Fe_3O_4 surface may also bond with the catechol groups of dopamine through dehydration [34]. TEM images in Fig. 2c–f display the well-defined core–shell structure of Fe_3O_4@PDA. As reported, the layer thickness of the polydopamine is a function of reaction time when other experimental parameters are fixed [25]. Thereby, the shell thickness can be readily tuned from 12 nm (Fig. 2c) to 24 nm (Fig. 2d) and 45 nm (Fig. 2e) by changing reaction time from 6 h to 12 h and 24 h, respectively. However, as the reaction time further increased to 48 h, the increase of thickness was not obvious (50 nm, Fig. 2f), indicating that the growth of PDA shell had reached its limit under this condition (2 mg mL^{-1} dopamine, pH 8.5, 10 mM Tris buffer) [35]. A compromise between experimental duration and PDA

thickness was made and the reaction time was set to be 24 h in all results presented below.

The core–shell structured Fe_3O_4@PDA–Au nanocomposites were obtained by adding the as-prepared Fe_3O_4@PDA to a $HAuCl_4$ solution and did not require extra reagents or thermo treatment. The possible mechanism of the generation and stabilization of Au NPs on PDA coating is speculated in Fig. 1. When Fe_3O_4@PDA NPs are mixed with $HAuCl_4$ solution, Au^{3+} ions diffuse into the PDA layer and then are reduced to Au^0 atoms *in situ* by the catechol groups of PDA and the catechol groups are oxidized to corresponding quinones simultaneously [27]. Subsequently, the neighboring Au^0 atoms cluster together to form Au NPs which are stabilized by the quinones and unoxidized catechol groups of PDA like other polyphenol compounds [36–38]. Here, the PDA serves as a reductant as well as a stabilizer which can help to prevent the Au NPs from agglomeration.

The impact of $HAuCl_4$ dosage on the size and amount of Au NPs immobilized in the PDA shell was investigated. Representative TEM images and the corresponding particle size distribution of Au NPs are presented in Fig. 3 and S3, respectively. The size and amount of the Au NPs show strong dependency on the dosage of $HAuCl_4$. When the concentration of $HAuCl_4$ is low (3×10^{-4} and 4.5×10^{-4} M), very few and large-size Au NPs are immobilized on the surface of PDA shell (Fig. 3a and b). As the concentration of $HAuCl_4$ increases to 6×10^{-4} M, plenty of monodisperse Au NPs with small size are both embedded in PDA shell and distributed on PDA surface (Fig. 3c). If the concentration of HAuCl4 further increases (9×10^{-4}, 12×10^{-4} M), Au NPs with wider size distribution and obvious agglomeration can be observed (Fig. 3d and e and Fig. S3d and e). To explain the above phenomenon, we presume that the formation of Au NPs stabilized by Fe_3O_4@PDA is a kinetic-controlled process. At a low dosage of $HAuCl_4$, the sparse Au^{3+} ions may only reach to the shell surface where the Au^{3+} ions were first reduced to Au^0 by the superficial catechol groups and then the Au^0 species aggregate to Au NPs. Possibly due to the groups in the surface is limited, the stabilization interactions between the PDA groups with Au NPs is somewhat weak, which leads to the growth of large-size Au NPs. As the dosage of $HAuCl_4$ increases, Au^{3+} ions will diffuse into the inner layer of the PDA shell. There are more abundant PDA groups in the inner shell than in the outside surface, which makes the stabilizing interactions in the inner shell stronger than those in the surface. Thus, the strong binding effect can undoubtedly suppress the growth of Au NPs, which results in the formation of smaller and well-distributed Au NPs. At even higher dosage of $HAuCl_4$, the PDA groups are not enough to efficiently stabilize the formed Au NPs. Consequently, the excess Au NPs agglomerate with other Au NPs. Considering the catalytic performance of Au NPs is greatly determined by their size and dispersity, 6×10^{-4} M of $HAuCl_4$ was selected to prepare the nanocatalyst, and the ICP result demonstrates that the loading amount of Au on Fe_3O_4@PDA@Au_6 is 4.3 wt.%.

Fig. 3f shows the XRD patterns of the Fe_3O_4, Fe_3O_4@PDA and Fe_3O_4@PDA–Au nanoparticles. All diffraction peaks in the black spectrum can be easily indexed as face-centered cubic Fe_3O_4, which matches well with the reported data (JCPDS card No. 19-629). The XRD patterns of the Fe_3O_4 with (red) and without PDA coating (black) exhibit similar features, which means that the amorphous PDA coating does not change the crystalline phase of Fe_3O_4. In the pattern of Fe_3O_4@PDA–Au (blue), three new peaks at 2θ of 38°, 43°, and 65° appear, which should be accordingly assigned to the (1 1 1), (2 0 0), and (2 2 0) lattice planes of the cubic phase Au (JCPDS card no. 04-784) and the characteristic peaks of Fe_3O_4 continue to be present. The elemental composition of Fe_3O_4@PDA–Au composite was determined by EDX. As shown in Fig. S4, the Au, Fe and O, C and N signals which are, respectively from Au, Fe_3O_4 and PDA appear in the EDX spectrum.

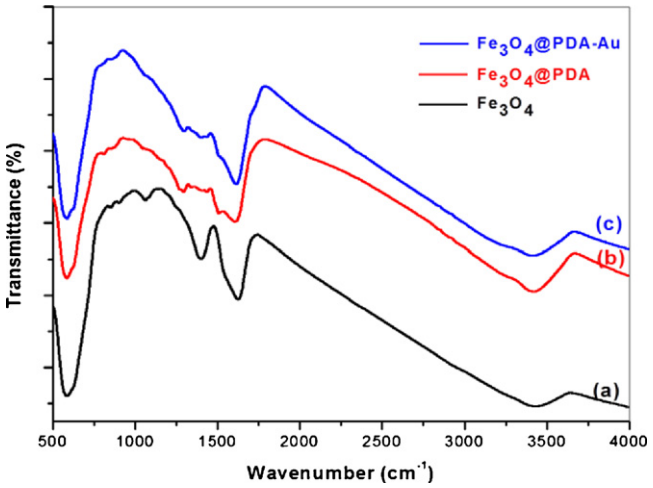

Fig. 4. FTIR spectra of the as-prepared Fe_3O_4 (a), Fe_3O_4@PDA (b), and Fe_3O_4@PDA–Au (c).

Fig. 4 presents the FTIR spectra of the Fe_3O_4, Fe_3O_4@PDA, and Fe_3O_4@PDA–Au nanocomposites. In the FTIR spectrum of pure Fe_3O_4 (Fig. 4a), the adsorption peak at 1403 cm^{-1} is related to the vibration of COO— groups modified on Fe_3O_4 surface, and the broad peak at 1626 cm^{-1} is corresponding to the vibration of overlapping COO— and O—H groups of Fe_3O_4 [39]. The peaks observed at 585 and 3430 cm^{-1} can be associated with Fe—O vibration and O—H stretching vibration, respectively [39]. For Fe_3O_4@PDA, in comparison with Fe_3O_4, the peaks of carboxylate group are covered and the bands at 1604 and 1508 cm^{-1} appear (Fig. 4b), which belong to the C=C stretching vibrations of aromatic ring [40]. Typical peak around 1290 cm^{-1} may be the primary amine vibration from the PDA coating.[40] In the spectrum of Fe_3O_4@PDA–Au, the peak intensities of aromatic ring decrease, and the peak at 1615 cm^{-1} is present due to the immobilized Au NPs (Fig. 4c).

To further confirm the presence of PDA–Au shell on the surface of Fe_3O_4 NPs, XPS was performed to provide elemental information of the surface atomic composition of various materials. Fig. 5a exhibits the XPS spectrum of Fe_3O_4@PDA–Au, which clear shows the signals for C, O, Au, and N element. Fig. 5b displays the high-resolution spectra for Au 4f. The binding energies at 83.0 and 86.6 eV are attributed to Au $4f_{7/2}$ and Au $4f_{5/2}$ of the Au^0. Furthermore, the binding energy at 710.2 eV for Fe 2p3 shown in Fig. S5 cannot be detected in the spectrum of Fe_3O_4@PDA–Au. These results provide supportive evidence that all the Fe_3O_4 cores in the composites are confined within a shell of PDA–Au, which are consistent with the above TEM, XRD, FTIR and EDX analyses.

The magnetic properties of various as-prepared magnetic nanoparticles were evaluated and Fig. 6 shows the M—H hysteresis loops of the nanocomposites measured by sweeping the external field between −1 and 1*T* at room temperature. All the three magnetization curves show no remanence and coercivity, suggesting the superparamagnetic behavior of each composite. The saturation magnetization value of Fe_3O_4@PDA (46.3 emu g^{-1}) is lower than Fe_3O_4 (62.3 emu g^{-1}) due to the existence of non-magnetic PDA coating. As for Fe_3O_4@PDA–Au, the saturation magnetization value further decreases to 39.6 emu g^{-1}, which can attribute to the loading of Au NPs on the surface of PDA shell and the consequently increasing thickness of the shell on the Fe_3O_4 NPs surfaces. However, the magnetic sensitivity of Fe_3O_4@PDA–Au is strong enough to provide an easy and effective way to separate the catalyst from reaction system. All the above results reveal the successful synthesis of the Fe_3O_4@PDA–Au composites.

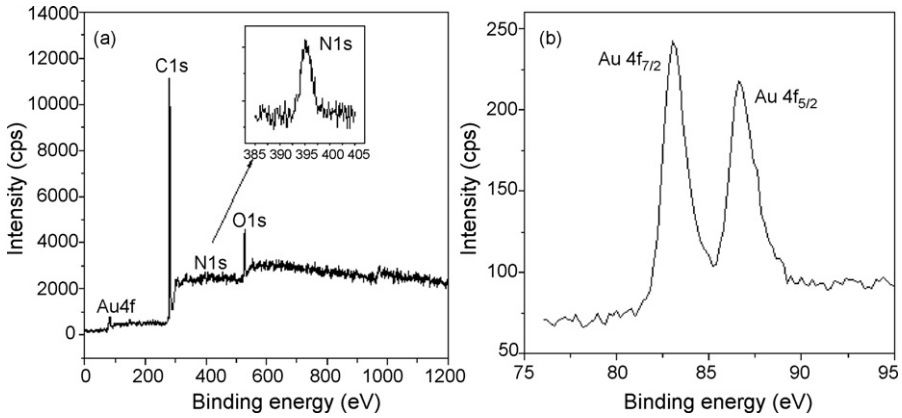

Fig. 5. XPS spectra of as-prepared Fe_3O_4@PDA–Au. (a) Survey scan spectrum. (b) Au 4f core-level spectrum. The inset in (a) shows N 1s core-level spectrum.

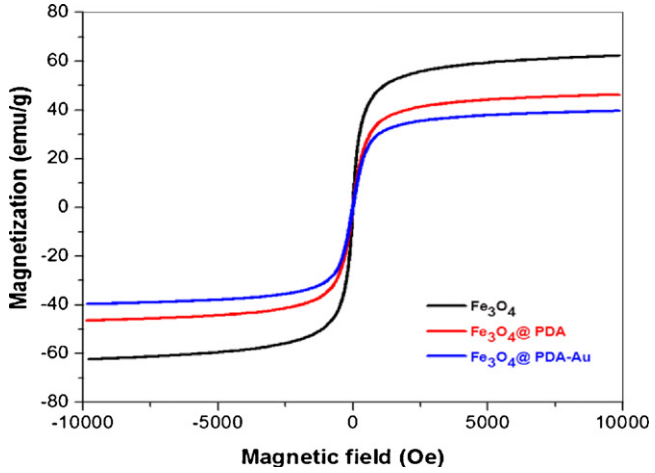

Fig. 6. Room-temperature magnetization hysteresis loops of the as-prepared Fe_3O_4 (a), Fe_3O_4@PDA (b) and Fe_3O_4@PDA–Au (c).

To check the catalytic capability of Fe_3O_4@PDA–Au nanocomposites, the reduction of *o*-nitroaniline (*o*-NA) to their corresponding daughter derivatives (benzenediamine) in the presence of $NaBH_4$ was chosen as a model reaction [41–43]. Fig. 7a shows the typical changes of UV–vis absorption spectra during the reaction with the characteristic peaks of *o*-NA at 412 and 282 nm. This reaction does not occur in absence of Fe_3O_4@PDA–Au catalysts during a period of more than two days. After the addition of a small amount of Fe_3O_4@PDA–Au composites, the absorbance at 412 nm successively decreases and nearly disappears at 7 min. At the same time, a shift of the peak from 282 nm to 289 nm can be observed. These indicate the gradual reduction of *o*-NA to benzenediamine under the catalysis of Fe_3O_4@PDA–Au nanocomposites. Control experiments, with bare Fe_3O_4 NPs and Fe_3O_4@PDA as catalyst instead of Fe_3O_4@PDA–Au, were also carried out. No obvious change in the absorbance can be detected even after 24 h, clearly demonstrating that the reduction of *o*-NA by $NaBH_4$ is solely catalyzed by the Au NPs stabilized on Fe_3O_4@PDA.

Since the concentration of $NaBH_4$ is higher than that of *o*-NA and can be considered as a constant during the reaction period, the rate constants for the reduction of *o*-NA is allowed to evaluate by the pseudo-first-order kinetics. The ratios of C_t (the concentration of *o*-NA at time t) to C_0 (the initial concentration of *o*-NA) were obtained from the relative intensity ratios of the respective absorbance (A_t/A_0) at 412 nm. To confirm the difference in catalytic performance of catalysts with different Au size and Au density, we have made a comparison of their catalytic reaction rates for *o*-NA. The linear relationships of $\ln(C_t/C_0)$ *versus* time (t) for these catalysts indicate that the reduction of *o*-NA follows the pseudo-first-order kinetics (Fig. 7b). The rate constants k estimated directly from the slope of the straight line in Fig. 7b are 0.24, 0.63, and 0.33 min^{-1} for the reactions catalyzed by Fe_3O_4@PDA–Au_3, Fe_3O_4@PDA–Au_6, and Fe_3O_4@PDA–Au_9 (subscript stands for the initial concentration of gold precursor salt, 1×10^{-4} M), respectively. This means that the Fe_3O_4@PDA–Au_6 nanocomposites show a much higher catalytic activity than others. Generally, the catalytic efficiency of Au NPs depends on the size, site density, stability, and

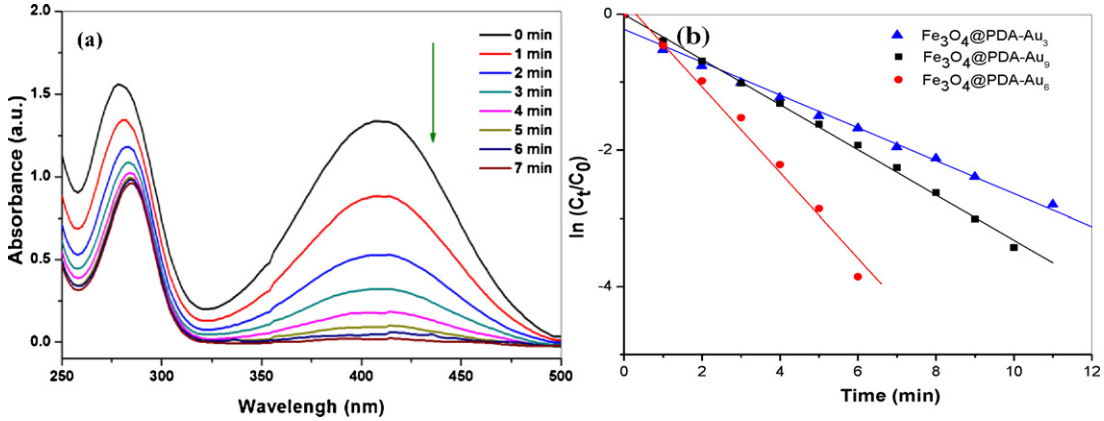

Fig. 7. (a) Time-dependent UV–vis absorption spectra of the *o*-nitroaniline reduced by $NaBH_4$ catalyzed by the Fe_3O_4@PDA–Au composites. (b) Plot of $\ln(C_t/C_0)$ *versus* time for different Fe_3O_4@PDA–Au catalysts.

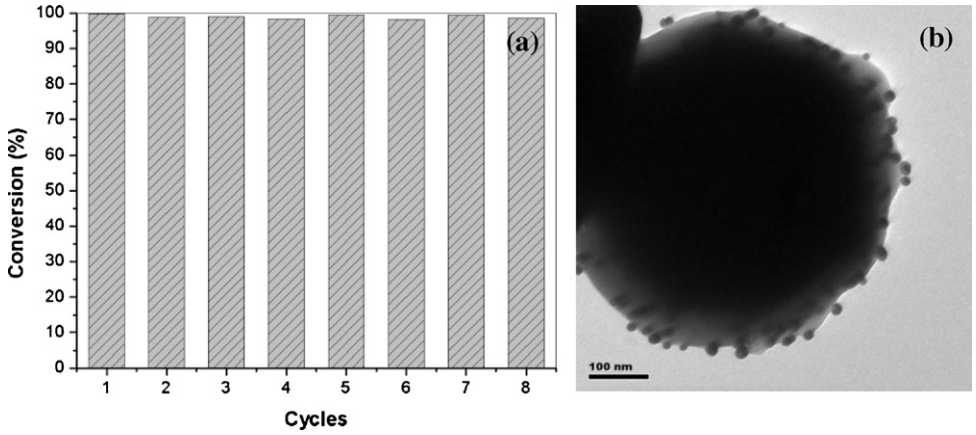

Fig. 8. (a) Conversion of *o*-nitroaniline in eight successive cycles with Fe_3O_4@PDA–Au catalyst. (b) TEM images of Fe_3O_4@PDA–Au catalyst after eight cycles.

gold–support interaction [44]. In this work, the different reduction rate should mainly attribute to the size and density effect of the Au NPs in the nanocatalysts. Compared with Fe_3O_4@PDA–Au_3 and Fe_3O_4@PDA–Au_9, more and smaller Au NPs can be observed in Fe_3O_4@PDA–Au_6 (see Fig. 3), which would significantly enhance the accessibility of *o*-NA to catalytic sites and thus elevate the catalytic performance. Hence, the dosage of $HAuCl_4$ plays an important role in controlling the formation of Au NPs and affects the catalytic activity greatly.

We have further investigated the catalytic activity of the as-prepared Fe_3O_4@PDA–Au catalyst for the reduction of other nitrobenzene analogs including nitroaniline, nitrophenol, nitrotoluene, and nitrochlorobenzene (Table 1). All the catalytic conditions of these analogs are same to that of *o*-NA and the reaction progresses of these nitrobenzenes were monitored by UV–vis spectrometry. The conversion was determined by the gas chromatography/mass spectroscopy (GC/MS) analysis of the residual nitrobenzene in the mixture after reaction. From Fig. S6, the typical change of UV–vis spectra of each compound during the reaction clearly demonstrates that the reduction of these nitrobenzenes did occur in the presence of a small amount of Fe_3O_4@PDA–Au catalyst. As shown in Table 1, our catalyst exhibits good catalytic activity with excellent yields toward a series of nitrobenzene compounds regardless of the types and position of the substituents. Three kinds of nitroaniline can be transformed within 7 min with a conversion of 99% and the effect of the substituent position is very small. Interestingly, when the catalyst was used to catalyze the reduction of nitrotoluene and nitrochlorobenzene, it showed a lower activity than those of nitroaniline and nitrophenol. The possible reason for this phenomenon is that the reaction processes of nitrotoluene and nitrochlorobenzene are more complicated than those of nitroaniline and nitrophenol. For example, the reduction of nitrotoluene and nitrochlorobenzene can produce amino and nitroso form products while nitroaniline and nitrophenol can only be converted into corresponding anilines in the presence of $NaBH_4$ and Au catalyst [45]. These results indicate the generality and the efficacy of our new catalyst toward the reduction of different nitrobenzene and we will do more works on the catalytic reaction mechanism of these nitrobenzenes in the future research. In addition, we also made a comparison of the catalytic performance of our catalyst with other catalysts (see Table S1). From Table S1 we can conclude that the Fe_3O_4@PDA–Au catalyst in the present work has a comparable conversion and a higher catalytic activity than those of most other catalysts. Thus, a simple and green preparation of a Fe_3O_4@PDA–Au catalyst with high catalytic efficiency was presented in our article.

The Fe_3O_4@PDA–Au catalyst was used repeatedly after being separated from the reaction mixture by using an external magnet to investigate the reusability. Fig. 8a shows the reusability of the Fe_3O_4@PDA–Au composites as a catalyst for the reduction of *o*-NA with $NaBH_4$. The catalysts can be successfully recycled because of the magnetic separation ability (complete separation within 30 s) and reused for eight successive cycles with a conversion of >98%. We have also conducted ICP–MS measurements and TEM observation to check the stability of the as-prepared catalyst in the catalytic

Table 1
Reduction of various nitrobenzenes using Fe_3O_4@PDA–Au catalyst[a].

Entry	Compound	Structure	Time/min	Conversion
1	*o*-Nitroaniline	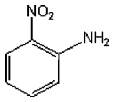	7	99%
2	*m*-Nitroaniline	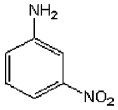	5	99%
3	*p*-Nitroaniline	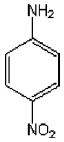	6	99%
4	*o*-Nitrotoluene	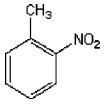	67	93%
5	*m*-Nitrotoluene	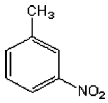	72	90%
6	*p*-Nitrophenol	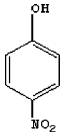	19	99%
7	*o*-Nitrochloro-benzene	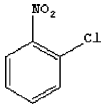	120	87%
8	2,4-Dinitrotoluene	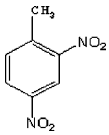	108	99%

[a] Reaction condition: 0.25 mL of 3.4×10^{-3} M nitrobenzene, 0.05 mL of 1 mg mL^{-1} catalyst, and 0.25 mL of 1.2 M fresh $NaBH_4$.

tests. The solid catalyst was separated from the reactant mixture after each catalytic cycle and the residual filtrate was digested and measured by ICP–MS to determine the lost amount of gold and iron. No Fe element was found in the residual filtrates, which suggests that the Fe_3O_4 NPs were well protected by the PDA shell. At the same time, only trace Au element can be detected in the residual filtrates and the Au content remained on the catalyst after each repeated catalytic process can be calculated from the Au concentration in each filtrate (Table S2). More than 83% of Au content was maintained on catalyst even after eight runs (Fig. S7b), which proved the good stability of the catalyst. The slight decrease in rate constant (Fig. S7a) can be originated from the negligible loss of Au and the adsorption of benzenediamine generated from the reduction reaction onto the surface of the Au NPs [46]. In addition, the TEM image of Fe_3O_4@PDA–Au nanocatalyst after eight cycles also shows that the structure and morphology are well maintained (Fig. 8b), which provides a supportive evidence for the good stability of the catalyst.

4. Conclusions

In summary, well-defined core–shell structured composites with Fe_3O_4 core coated by a PDA–Au shell have been successfully synthesized. In this process, the PDA coating acts as both reductant and stabilizer without the necessity for additional reagents and heat treatment. The size of Au NPs and the thickness of PDA shell can be easily controlled by varying the dosage of $HAuCl_4$ and the reaction time, respectively. The synthesized Fe_3O_4@PDA–Au nanocatalysts show high catalytic activity and excellent recyclability in the reduction of nitrobenzne. Furthermore, this simple, low-toxic and low-cost method might be extended for the preparation of other magnetic nanocatalysts for practical application in more interesting reactions.

Acknowledgements

We thank the National Basic Research Program of China (2011CB936001) and the National Natural Science Foundation of China (20975110, 21277152, 21277002) for financial support.

Appendix A. Supplementary data

Supplementary data associated with this article can be found, in the online version, at doi:10.1016/j.apcatb.2012.12.037.

References

[1] P.K. Jain, X. Huang, I.H. El-Sayed, M.A. El-Sayed, Accounts of Chemical Research 41 (2008) 1578–1586.
[2] C. Noguez, I.L. Garzon, Chemical Society Reviews 38 (2009) 757–771.
[3] Y. Denkwitz, M. Makosch, J. Geserick, U. Hormann, S. Selve, U. Kaiser, N. Husing, R.J. Behm, Applied Catalysis B: Environmental 91 (2009) 470–480.
[4] D. Sebastian, A.G. Ruiz, I. Suelves, R. Moliner, M.J. Lazaro, V. Baglio, A. Stassi, A.S. Arico, Applied Catalysis B: Environmental 115 (2012) 269–275.
[5] T.A. Zepeda, A. Martinez-Hernandez, R. Guil-Lopez, B. Pawelec, Applied Catalysis B: Environmental 100 (2010) 450–462.
[6] J. John, E. Gravel, A. Hagege, H.Y. Li, T. Gacoin, E. Doris, Angewandte Chemie International Edition 50 (2011) 7533–7536.
[7] P.-P. Fang, A. Jutand, Z.-Q. Tian, C. Amatore, Angewandte Chemie International Edition 50 (2011) 12184–12188.
[8] A. Villa, C.E. Chan-Thaw, L. Prati, Applied Catalysis B: Environmental 96 (2010) 541–547.
[9] A. Baylet, C. Capdeillayre, L. Retailleau, J.L. Valverde, P. Vernoux, A. Giroir-Fendler, Applied Catalysis B: Environmental 102 (2011) 180–189.
[10] M. Zhao, L. Sun, R.M. Crooks, Journal of American Chemical Soceity 120 (1998) 4877–4878.
[11] B. Fei, B. Qian, Z. Yang, R. Wang, W. Liu, C. Mak, J. Xin, Carbon 46 (2008) 1795–1797.
[12] Y. Tai, W. Yamaguchi, M. Okada, F. Ohashi, K. Shimizu, A. Satsuma, K. Tajiri, H. Kageyama, Journal of Catalysis 270 (2010) 234–241.
[13] G. Zhao, M. Ling, H. Hu, M. Deng, Q. Xue, Y. Lu, Green Chemistry 13 (2011) 3088–3092.
[14] Y.H. Deng, Y. Cai, Z.K. Sun, J. Liu, C. Liu, J. Wei, W. Li, C. Liu, Y. Wang, D.Y. Zhao, Journal of American Chemical Soceity 132 (2010) 8466–8473.
[15] R.L. Oliveira, P.K. Kiyohara, L.M. Rossi, Green Chemistry 12 (2010) 144–149.
[16] F. Chen, Q. Chen, S. Fang, Y. Sun, Z. Chen, G. Xie, Y. Du, Dalton Transaction 40 (2011) 10857–10864.
[17] Y. Zhu, J. Shen, K. Zhou, C. Chen, X. Yang, C. Li, Journal of Physical Chemistry C 115 (2011) 1614–1619.
[18] J. Ge, Q. Zhang, T. Zhang, Y. Yin, Angewandte Chemie International Edition 47 (2008) 8924–8928.
[19] M. Scampicchio, J. Wang, A.J. Blasco, A. Sanchez Arribas, S. Mannino, A. Escarpa, Analytical Chemistry 78 (2006) 2060–2063.
[20] J.A. Jacob, H.S. Mahal, N. Biswas, T. Mukherjee, S. Kapoor, Langmuir 24 (2007) 528–533.
[21] X. Huang, X.P. Liao, B. Shi, Green Chemistry 13 (2011) 2801–2805.
[22] Y. Lee, T.G. Park, Langmuir 27 (2011) 2965–2971.
[23] H. Lee, N.F. Scherer, P.B. Messersmith, Proceedings of the National Academy of Sciences of the United States of America 103 (2006) 12999–13003.
[24] H. Lee, Y. Lee, A.R. Statz, J. Rho, T.G. Park, P.B. Messersmith, Advanced Materials 20 (2008) 1619–1623.
[25] H. Lee, S.M. Dellatore, W.M. Miller, P.B. Messersmith, Science 318 (2007) 426–430.
[26] M. Sureshkumar, D.Y. Siswanto, C.K. Lee, Journal of Materials Chemistry 20 (2010) 6948–6955.
[27] K.C.L. Black, Z. Liu, P.B. Messersmith, Chemistry of Materials 23 (2011) 1130–1135.
[28] Y. Fu, P. Li, Q. Xie, X. Xu, L. Lei, C. Chen, C. Zou, W. Deng, S. Yao, Advanced Functional Materials 19 (2009) 1784–1791.
[29] R.P. Liang, X.Y. Meng, C.M. Liu, J.D. Qiu, Electrophoresis 32 (2011) 3331–3340.
[30] A.-J. Wang, H.-Y. Cheng, B. Liang, N.-Q. Ren, D. Cui, N. Lin, B.H. Kim, K. Rabaey, Environmental Science and Technology 45 (2011) 10186–10193.
[31] A. Latifoglu, M.D. Gurol, Water Research 37 (2003) 1879–1889.
[32] J. Liu, Z.K. Sun, Y.H. Deng, Y. Zou, C.Y. Li, X.H. Guo, L.Q. Xiong, Y. Gao, F.Y. Li, D.Y. Zhao, Angewandte Chemie International Edition 48 (2009) 5875–5879.
[33] J. Si, H. Yang, Materials Chemistry and Physics 128 (2011) 519–524.
[34] J.L. Dalsin, L.J. Lin, S. Tosatti, J. Voros, M. Textor, P.B. Messersmith, Langmuir 21 (2005) 640–646.
[35] F. Bernsmann, V. Ball, F.d.r. Addiego, A. Ponche, M. Michel, J.J.d.A. Gracio, V.r. Toniazzo, D. Ruch, Langmuir 27 (2011) 2819–2825.
[36] X. Huang, H. Wu, X. Liao, B. Shi, Green Chemistry 12 (2010) 395.
[37] P. Tripathy, A. Mishra, S. Ram, H.J. Fecht, J. Bansmann, R.J. Behm, Nanotechnology 20 (2009) 075701.
[38] H. Wu, X. Huang, M.M. Gao, X.P. Liao, B. Shi, Green Chemistry 13 (2011) 651–658.
[39] J. Liu, Z. Sun, Y. Deng, Y. Zou, C. Li, X. Guo, L. Xiong, Y. Gao, F. Li, D. Zhao, Angewandte Chemie International Edition in English 48 (2009) 5875–5879.
[40] M. Sureshkumar, C.K. Lee, Carbohydrate Polymers 84 (2011) 775–780.
[41] L. Tan, D. Chen, H. Liu, F. Tang, Advanced Materials 22 (2010) 4885–4889.
[42] J. Huang, L. Zhang, B. Chen, N. Ji, F. Chen, Y. Zhang, Z. Zhang, Nanoscale 2 (2010) 2733–2738.
[43] Y. Yang, J. Liu, X. Li, X. Liu, Q. Yang, Chemistry of Materials 23 (2011) 3676–3684.
[44] L. Chen, J. Hu, R. Richards, Journal of American Chemical Soceity 131 (2008) 914–915.
[45] D.M. Dotzauer, S. Bhattacharjee, Y. Wen, M.L. Bruening, Langmuir 25 (2009) 1865–1871.
[46] F.-h. Lin, R.-a. Doong, Journal of Physical Chemistry C 115 (2011) 6591–6598.